Article:
Chen, H, Ye, S orcid.org/0000-0001-5152-5753, Tao, Q et al. (3 more authors) (2021) Hygroresponsive Torsional Yarns and Actuators Based on Cascade Amplification of the Deformation. Macromolecular Materials and Engineering, 306 (5). 2000822. ISSN 1438-7492

https://doi.org/10.1002/mame.202000822

Hygroresponsive Torsional Yarns and Actuators based on Cascade Amplification of the Deformation

*Hui Chen, Sunjie Ye, Qianyi Tao, Zhuang Chen, Yingfeng Tu, and Xiaoming Yang**

H. Che, Q. Tao, Z. Chen, Prof. Y. Tu, Prof. X. Yang
State and Local Joint Engineering Laboratory for Novel Functional Polymeric Materials, Suzhou Key Laboratory of Macromolecular Design and Precision Synthesis, Department of Polymer Science and Engineering, College of Chemistry, Chemical Engineering and Materials Science
Soochow University
Suzhou 215123, P. R. China.
E-mail: yangxiaoming@suda.edu.cn
Dr. S. Ye
School of Physics and Astronomy, University of Leeds, LS2 9JT, Leeds, UK.

Keywords: Torsional actuator; Moisture-triggered actuation; Self-twisted yarn; Water transport; Intelligent textile

Fiber-based hygroresponsive torsional actuators provide desirable merits, such as light weight and shapeability, for developing smart systems to harvest energy from moisture which is a ubiquitous natural resource. A key challenge in this development is to realize moisture-triggered actuation combining large actuation and rapid responses. Here, a multi-scale design strategy has been explored to create high-performance hygroresponsive torsional actuators consisting of chitosan and multiwalled carbon nanotubes (MWCNTs). The superior actuation performance arises from the synergism of contributing factors at different scales, including (1) MWNCTs accelerate the water transport in primary twisted fibers (PTFs), fostering the rotation of PTFs upon moisture stimuli; (2) in-situ formed hierarchically-assembled twists realize cascade amplification of moisture-triggered actuation. Specifically, PTFs are self-twisted to generate secondary helical yarns, that are subsequently over-twisted to yield tertiary coiled yarn. The resultant yarn actuator can reach a maximum rotation speed of 11400 rpm in 5s, output gravitational potential energy of 2.4 J kg^{-1} and gravitational potential power of 0.053 W kg^{-1} during contraction. This work represents the first design of fiber-based actuators by virtue of moisture-triggered in-situ formation of yarns. The established principles of multiscale design will enable high-performance fiber-based hygroresponsive actuators towards advanced intelligent textile and soft robotics.

1. Introduction

Converting the energy contained in the natural humidity/moisture/water into mechanical energy by actuators hold potential to contribute to addressing global challenges of energy crisis. In nature, water can trigger movements in living systems as an environmental stimulus [1-4]. These movements arise from the expand and contract of the water molecules fluid in the plant upon water absorption and deabsorption [5,6]. Among different kinds of movements (such as bending, contraction, stretching and twisting) [7], torsional movements of the plant have attracted widespread interest, such as the twisting of wood cells Plaza [8], coiling of awns and helical motion of tendrils [9,10]. They are produced by distinctive swelling or shrinkage in hierarchically assembled structures of cellulose microfibrils in response to the humidity variation [11,12]. Motivated by torsional motions in plants, several hygroresponsive fiber-based torsional actuators have been investigated, owing to their twisted structures that can store and release energy, coupled with other desirable properties, such as light weight, miniaturization, and shapeability. Despite remarkable progress in this research direction [13], it remains a challenge to develop fiber-based hygroresponsvie torsional actuators that integrates large actuation and rapid response.

It was reported that, carbon nanotubes (CNTs)-based actuating fibres that responsive to solvent (ethanol, acetone, toluene and dichloromethane) can be fabricated via the hierarchical and helical assembly of CNTs forest [14-16]. The nano- to micro- scale gaps contributed to the fast response and big actuation. However, due to the hydrophobic property of pristine CNTs, limited actuation can be generated upon water-related stimuli (such as moisture), which are more widely accessible [14-17]. Our recent work on hygroresponsive bending actuators of chitosan (CS) /multiwall carbon nanotube (MWCNT) composite film reveals that, water transport facilitated by carbon nanotubes can enhance the amplitude and speed of the bending deformation of the film in response to the change of ambient humidity [18,19]. These together

have inspired our innovative multi-scale design of high-performance CS/MWCNTs yarn-based hydroresponsive torsional actuators.

In this work, primary twisted fibers (PTFs) were first fabricated by a traditional wet spinning and directly twisting method. Upon the moisture stimulus, a bundle of PTFs were self-twisted to form secondary helical yarn (SHY), that was next self-folded in the middle and over-twisted to eventually form tertiary coiled yarn (TCY). Consequently, a large and reversible rotation with a speed as high as 11400 rpm was achieved, coupled with a reversible contraction. Such a superb actuation benefits from the fast transport of water molecules provided by MWCNTs [20,21], the excellent swelling and deswelling behavior of the CS [22], alongside the hierarchically-twisting process. Notably, distinct from reported yarn-based hydroresponsive torsional actuators [23], our actuators have SHY and TCYs being in-situ formed upon the moisture stimulus of PTFs. This dynamic change leads to the cascade amplification of the deformation, thus inducing more sufficient and efficient actuation.

2. Results and discussion

2.1. Fabrication and Structure of the CS/MWCNTs PTFs

Figure 1 shows the schematic illustration of the fabrication process of the CS/MWCNTs PTFs. The two ends of the gel fiber obtained by spinning process (Figure 1a) were fixed on a twisting machine with a fixed end and a free rotating end (Figure 1b). The continuous twisting process was depicted in Figure 1b and Video S1) depicted a continuous PTFs with S twist (a left-handed yarn) and Z twist (a right-handed yarn). During the twisting process, the intrinsic structure of the gel fiber transformed from a random state to a more ordered state, leading to a decrease in entropy and the accumulation of more energy [23]. PTFs with different twist densities (1000~5000 turns m^{-1}) were prepared by adjusting twist conditions of the twisting machine. Figure 1c showed a typical scanning electron microscopy (SEM) image of a S-twisted PTFs with different twist densities. The fiber displayed a helical configuration upon the twisting

process. In addition, it can be seen from the cross-sectional images of twisted fiber in (Figure S1), the MWCNTs inside the fiber body were densely packed along the axial direction. In contrast, CS fiber showed smooth cross section. During the twisting process, the total length gradually reduced, while the diameter of the raw fiber increased, as water was continually extruded. (Figure 1d).

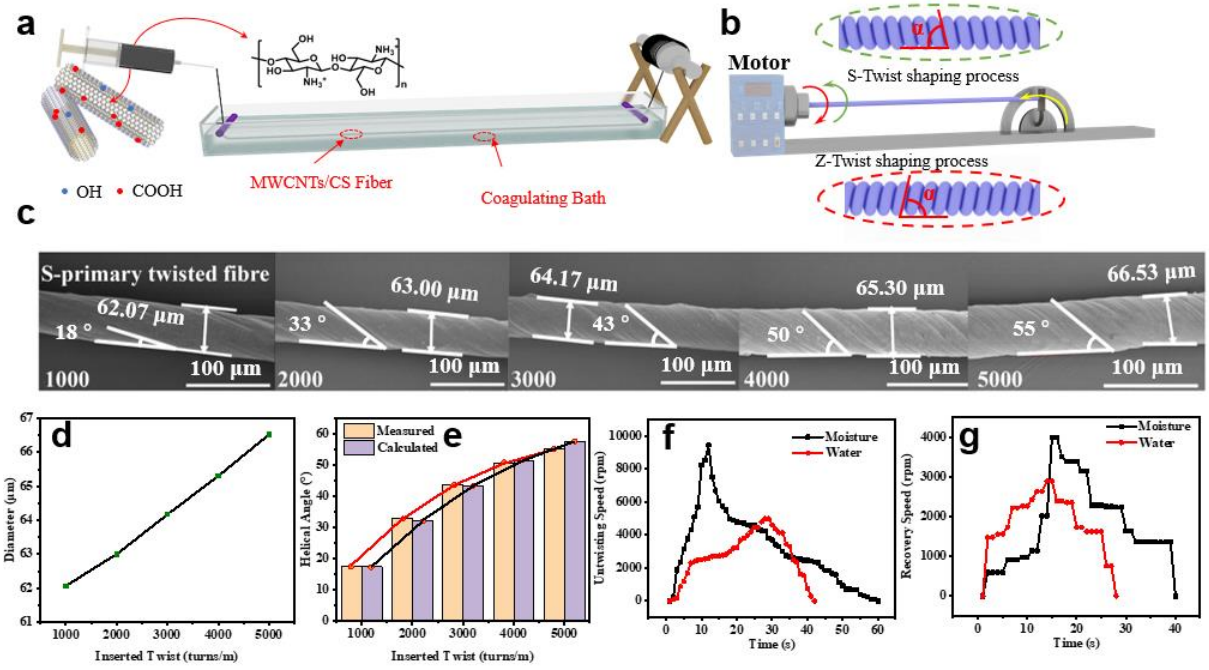

Figure 1. Schematic illustration of the wet spinning a) and twisting process b) of the gel fiber. c) SEM images of PTFs with varying twist densities: 1000, 2000, 3000, 4000, and 5000 turns m−1, shown from left to right. d) Diameter of PTFswith varying twist densities. e) Theoretical and experimental value of twist angles (α) of PTFFs with varying twist densities. Plot of the speed of f) untwisting and g) recovery rotation of PTFs as a function of time upon the stimulus of water or moisture.

By increasing the inserted twists, the distortion of the PTFs substantially increased, as evidenced by the amplification of the twist angle (α). The experimental value of α represents the angle between the axial direction of fiber and the twist direction of the fiber surface (Figure 1b and Figure 1c). The theoretical value of α can be calculated according to Equation (1) [24,25]:

$$\alpha = \tan^{-1}\left(2\pi rT\right) \qquad (1)$$

where r represents the fiber radius, T represents the number of twists per meter of the primary fiber. Unless otherwise indicated, both r and α were measured by SEM microscopy on fiber that were two-end-tethered under tension to prohibit untwist (Figure 1c). The results in (Figure 1e) showed that the experimental and theoretical values of α were in good agreement [26].

The PTFs exhibited remarkable torsional stroke triggered by liquid water or moisture. Figure 1f and Figure 1g show the rotation speed of PTFs upon the stimulus of liquid water and moisture, suggesting the maximum speed of untwisting and recovery stimulated by liquid water was smaller than that under moisture stimulus. Furthermore, liquid water caused a shorter rotation process (Figure 1f and Figure 1g). This was mainly due to the penetration and evaporation of liquid water being much slower than that of moisture. Thus, in this study, moisture instead of liquid water was used as stimulus without specified.

2.2. Actuating performance of PTFs

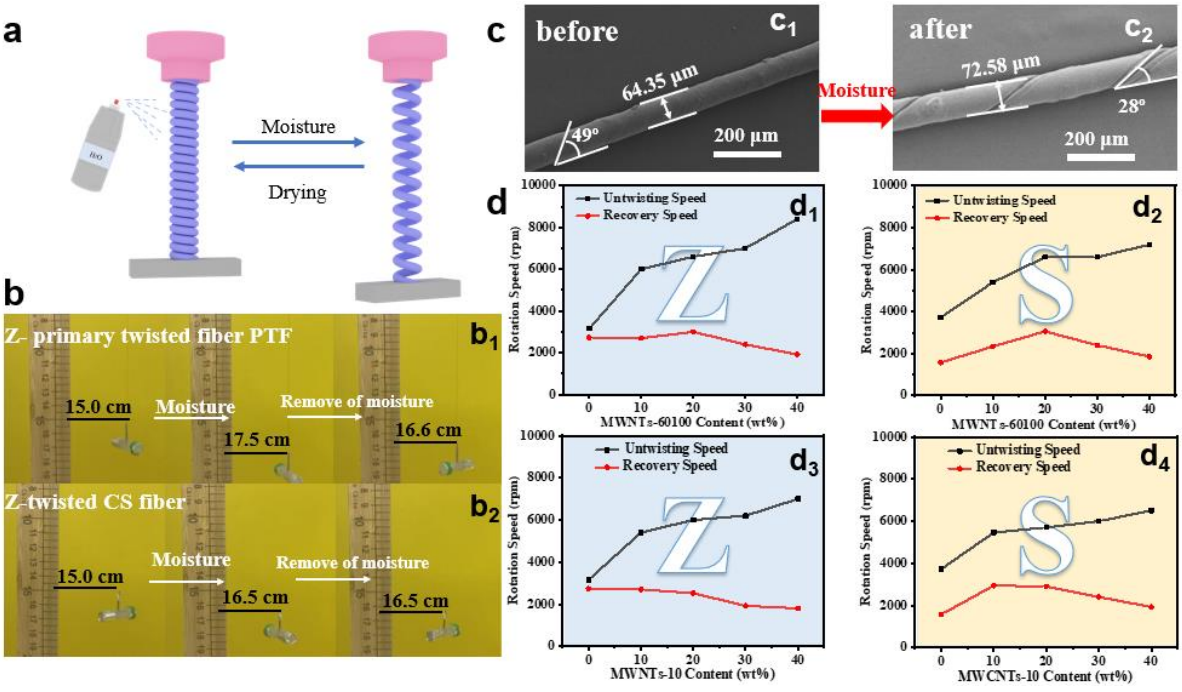

Figure 2. a) Schematic illustration of the reversible rotation of PTFs upon moisture stimulus. b) Left: elongation (moisture stimulus resulted in the untwisting deformation) and Right: recovery (water evaporation resulted the recovery of PTFs b_1) and CS fiber b_2) during the rotational motion. c) SEM images of PTFs before and after the moisture-triggered rotation. d)

Rotation speed of the PTFs versus contents of MWCNTs with different twisting directions: Z-PTFs with 60~100 nm MWCNTs d_1); S-PTFs with 60~100 nm MWCNTs d_2); Z-PTFs with 10 nm MWCNTs d_3); S-PTFs with 10 nm MWCNTs d_4).

During the tests of actuating performance of PTFs, one end of the actuator was fixed on a cantilever, and the other end was loaded with a paddle to straighten the fiber (**Figure 2a and Figure 2b**). The mass of the paddle is 1.14 g, which is approximately 1572 times larger than that of the fiber actuator. The actuated rotation was recorded with high-speed camera system. A frame-by-frame analysis was performed to extract quantitative results from the recorded video.

Owing to the hydrophilic properties of CS, excellent water transportation ability of MWCNTs [18], and the helical geometry of hybrid fiber, the fast and reversible swelling/shrinking of CS chains will happen with water molecules in and out, which could accordingly cause reversible torsional rotation and elongation of the PTFs (Figure 2b and Video S2, Supporting Information). The hybrid twisted fiber performed a (17.5-15)/15×100%=17% expansion along the axis (Figure 2b_1). The untwisted PTFs partly returned to its original state upon the moisture evaporation. However, the expansion was only 10% for twisted CS fibers. After the moisture has evaporated, the untwisted CS fiber cannot return to its original state, which confirm that the MWCNTs played a vital role in the transport of water molecules in the hybrid materials.

Figure 2 shows SEM images of PTFs before and after the moisture-triggered rotation. For a twisted fiber with an initial α of 49°, the value of α decreased to approximately 28° upon the moisture exposure (Figure 2c). This untwisting rotation of PTFs arise from the volumetric expansion of CS upon the adsorption of water molecules. We set the length of PTFs to be 20 cm and the twist number to be 3000 turns/m fordeterminnng the effects of the content of MWCNTs, the diameter of MWCNTs, and the twisted direction on the rotation speed of PTFs (Figure 2d). Upon the moisture stimulus, a paddle attached to the end point of a S-twist or Z-

twist fiber rotated in the clockwise or counter clockwise direction, respectively. The untwisting speed of the PTFs kept increasing as the MWCNTs concentration increased from 10 to 40 wt %, while the recovery speed almost kept unchanged with the increase of the MWCNTs concentration. This was because that water molecules were infiltrated into the PTFs more rapidly at a higher MWCNTs concentration, while the speed of water evaporation from the fiber to the environment was relatively small and almost unchanged with different MWCNTs concentration, leading to a smaller and unchanged recovery speed by varying MWCNTs concentrations. However, increasing the content of MWCNTs up to 40% caused poor processability. In addition, the diameter of MWCNTs also affected the rotation speed of PTFs. The PTFs with larger diameter (60~100 nm) of MWCNTs can adsorb and transport more water molecules than that of PTFs with smaller diameter of MWCNTs (10 nm), giving rise to a larger swelling force, thus inducing a larger untwisting speed (Figure 2d_1-2d_4). Interestingly, Z twisted fiber showed higher untwisting speed than that of S twisted fiber. The reason was still under investigation [27]. In this work, the actuation performance of Z twist hybrid fiber with 10% MWCNTs of 60~100 nm diameter was studied in detail in the following study.

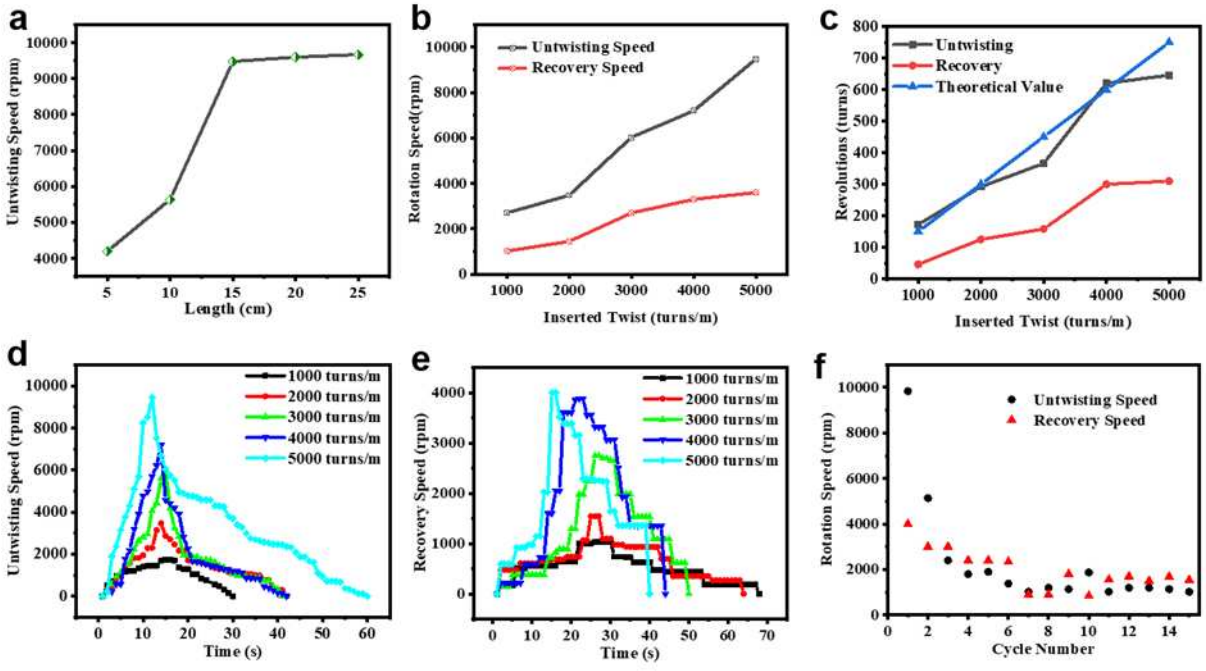

Figure 3. a) Untwisting speed of PTFs versus different exposed lengths when stimulated by moisture. b) Rotation speed of PTFs with different twist densities (from 1000 to 5000 turns/m) during untwisting and recovery processes. c) Revolutions of PTFs with different twist densities. Rotation speed of PTFs with varying twist versus time during d) untwisting and e) recovery processes. f) Cyclic stability test of the PTFs under periodic moisture stimulus.

The untwisting speed showed a linear increase when the fiber length varied from 5 to 15 cm, while kept constant as the fiber length increased from 15 to 20 cm (**Figure 3a**). This was because the driving force of untwisting enhanced with the increase of fiber length which corresponded to larger number of twists, and reached a plateau when the fiber length was above a critical value. In the following study, fiber with 15 cm was chosen for investigating the rotation speed in detail without specific clarification. The untwisting speed increased with the increase of inserted twists from 1000 to 5000 turns/m, indicating that larger inserted twist caused bigger energy storage during the twisting process (Figure 3b). However, the recovery revolutions (Figure 3c) were smaller than the untwisting revolution, due to elongation of untwist fiber and incomplete recovery to its original state. Increasing the inserted twists to larger than 5000 turns/m caused the breakage of fibers.

Figure 3d and e showed the rotational speed of the PTFs with different inserted twists as a function of time during the untwisting and recovery processes. PTFs with 5000 turns/m exhibited the best actuation performance due to the largest energy storage during the twisting process. The PTFs with 5000 turns/m reached a maximum untwisting speed of 9480 rpm in 12 s, and the entire untwisting process was completed in 60 s upon moisture stimulus. The maximum rotation speed was larger than twice of the value previously reported for hierarchically assembled helical fibers of MWCNTs upon alcohol stimulus.14 Furthermore, the comparation of rotational speed of PTFs and fiber-based actuators in literature (Table S1, Supporting Information) showed that, the actuating performance of the PTFs is superior to most of the reported systems. Additionally, the recovery speed of the PTFs with 5000 turns/m

reached a maximum value of 4000 rpm in 15 s, which was much slower than the untwisting speed. This may be because the desorption ability of water molecules was poorer than that of the absorption of water.

The energy harvesting behavior of a PTFs actuator was investigated with a length of 15 cm and a weight of 0.725 mg, which was loaded with a paddle with a weight of 1.14 g, a length of 24.58 mm, as well as a width of 7.64 mm. After stimulated by moisture, the paddle was accelerated to maximum angular speed (ω) of 993 rad s^{-1} in a short period of 12 s, with an average acceleration of 116 rad s^{-2}. Since the moment of inertia J was measured to be 1.784×10^{-8} kg m^{-2}, the maximum star-up torque was calculated to be 2.069×10^{-6} N m. The star-up torque provided a large peak power output of 3343 and 2080.45 W kg^{-1} for the whole process (60 s) (Equation 2). *W* was calculated by the equation of 3. The peak energy output and the whole energy output (60 s) were 40118.7 and 124827 J kg^{-1}, respectively.

$$P = J\omega^2/2t \qquad (2)$$

$$\mathrm{w} = \frac{1}{2}J\int \omega^2 dt \qquad (3)$$

The cyclic test upon the moisture stimulus revealed that, the actuation performance of the PTFs was unstable, with the rotation speed exhibiting obvious downward trend after one cycle (Figure 3f). The poor reversibility and repeatability of PTFs was caused by the swelling of liquid water that had destroyed the helical structures of PTFs in the first cycle.

Improving the cycling stability was essential for exploring the uses of fiber actuator. Hierarchical arrangement of a bundle of primary fibres together was a promising strategy to increase the actuating performance of torsional actuator [28,29]. Unfortunately, twisting a bundle of primary gel-state fibers or PTFs would cause the breakage of yarn. In this study, self-overtwisting strategy was used to prepare self-balanced tertiary coiled yarn (TCY).

2.3. Actuating performance of tertiary coiled yarn (TCY)

A bundle of PTFs can be self-twisted under moisture stimulus to form secondary helical yarn (SHY) (**Figure 4a**). Once the twisting degree reaches a critical value, SHY can over-twist and self-fold at the middle to form TCY (Figure 4a and Video S3, Supporting Information). In other words, the bundle of PTFs were self-twisted along the long axis of the yarn to form SHY with chirality of spiral opposite to the PTF's twisting direction that is S-twisted. Then, SHY was self-folded at the middle with Z-twist to form TCY. That is, the self-twisting direction was the opposite of the initial twisting direction, while the over-twisting direction was the same as the initial twisting direction (Figure 4a).

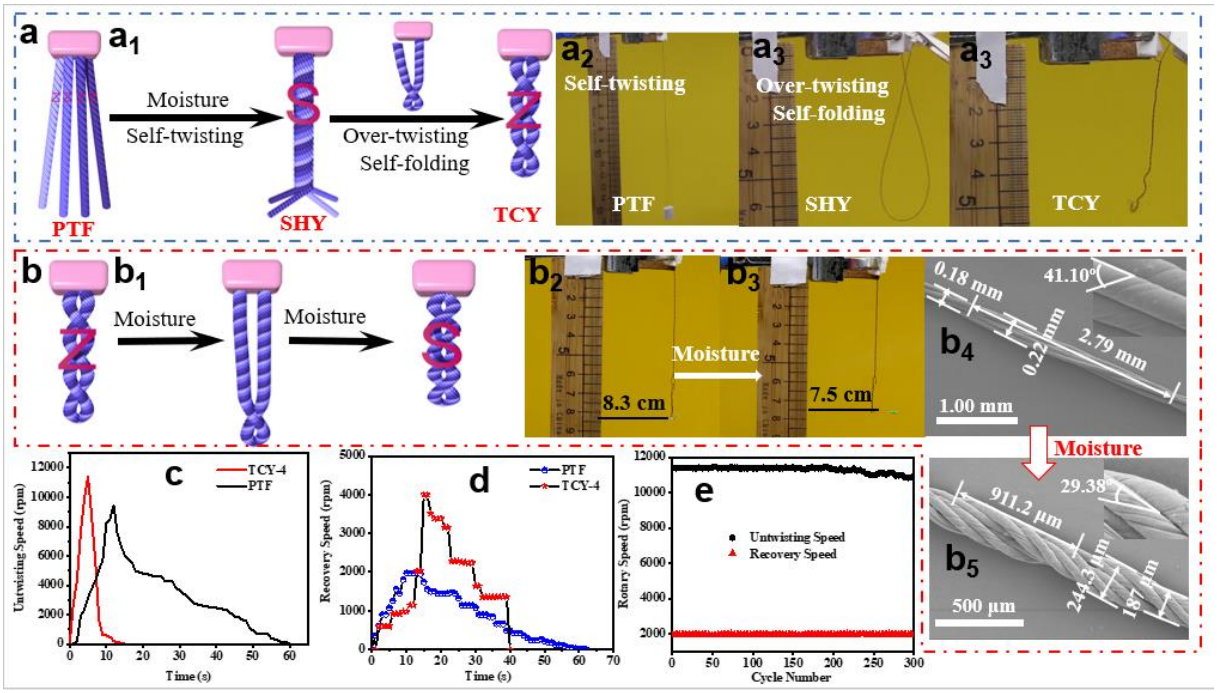

Figure 4. a) Schematic of the self-overtwisting strategy for preparation of TCY-4 a_1). Optical image of the self-overtwisting strategy a_2-a_3). b) Schematic illustration and optical images of the rotation and contraction of TCY-4 under moisture stimulus b1-b3). SEM image of TCY-4 before and after the moisture stimulus b_4-b_5). c) Rotation speed of TCY-4 and PTFS as a function of time during untwisting c) and recovery d) processes. e) Cyclic stability test of the TCY-4 under periodic moisture stimuli.

Different from PTFs, the TCYs showed contraction in length and swelling in fiber diameter after moisture stimulus (Figure 4b_2 and 4b_3) [30]. In order to investigate the effects of the unit usage on the manufacture process and torsional features of TCY, a series of fiber actuators ranging from 2 to 10 ply PTFs were prepared (Figure S2, Supporting Information). The contraction ratio of TCY increased with the increase of the amount of fiber, and reached the maximum value at 4 stocks (Figure S2a, Supporting Information). The diameter of TCY increased after the moisture stimulus as shown in (Figure 4b_4 and Figure 4b_5). The rotation speed-ply graph (Figure S2b, Supporting Information) showed that the rotation speed of TCY increased with the increase of the amount of fiber from 2 ply to 4 ply, while decreased with further increase of the amount of fiber from 4 ply to 10 ply. The time taken by the fiber actuator to reach the maximum speed increased with larger amount of fibers (Figure S2b, Supporting Information). TCY-4 which showed the optimal actuation performance was investigated in detail without specified clarification in the following study.

Figure 4c and Figure 4d presented the rotation and recovery speed of TCY-4 actuator with the load. As the water infiltration went on, the amount of water inhaled in the actuator was gradually becoming saturated, the swelling and contraction of TCY also would reach equilibrium (Video S4, Supporting Information). Consequently, after a period of rotation, the rotation of the actuator gradually slowed down until it stops. The untwisting speed is 11140 rpm, larger than that of PTFs (9480 rpm). Interestingly, the acceleration speed of TCY was also higher than that of PTFs (Figure 4d). However, the recovery speed of TCY was as slow as 2000 rpm and the whole recovery process lasted for 60 s. The porous feature of the hybrid yarns and the multiscale gaps (Figure 4b_5) were supposed to enable rapid adsorption and transportation of water molecules [14]. the recovery speed was still low due to the slow desorption of water molecules.

It was found from the SEM image of TCY-4 (Figure 4b4 and Figure 4b5) that, upon the moisture stimulus, the twist angle of TCY decreased from 41.19° to 29.38°, the dimeter increased from 220 μm to 244.3 μm, and the pitch decreased from 2790 μm to 911.2 μm. We investigated the actuating behavior of TCY-4 actuator with a length of 7 cm and a mass of 2.9 mg, which was loaded with a paddle of 1.029 g in weight, 3.80 mm in length and 1.50 mm in width. Under the moisture stimulus, the paddle was accelerated to maximum angular speed of 1197 rad s^{-1} in a short period of 5 s, with an average acceleration of 350 rad s^{-2}. The moment of inertia J was measured to be 0.4348×10^{-8} kg m^{-2}, the maximum star-up torque was calculated to be1.52×10^{-6} N m. The star-up torque provided a high peak power output of 221.2 W kg^{-1} and 233.6 W kg^{-1} for the whole process (15 s). The peak energy output and the whole energy output (15 s) were 1105.9 J kg^{-1} and 3503.7 J kg^{-1}, respectively. At the same time, the TCY-4 actuator (0.0522 g) lifted a reflector of 1.0238 g in 12 s, delivering an additional gravitational potential power output (E_k) of up to 11.35 Wkg^{-1} and energy output is 45.4 J kg^{-1}. The energy output by the TCY-4 was several orders of magnitude higher than that previously achieved by a twisted GO fiber [24].

2.4. Energy storage and conversion of the TCY and its potential application in smart textile

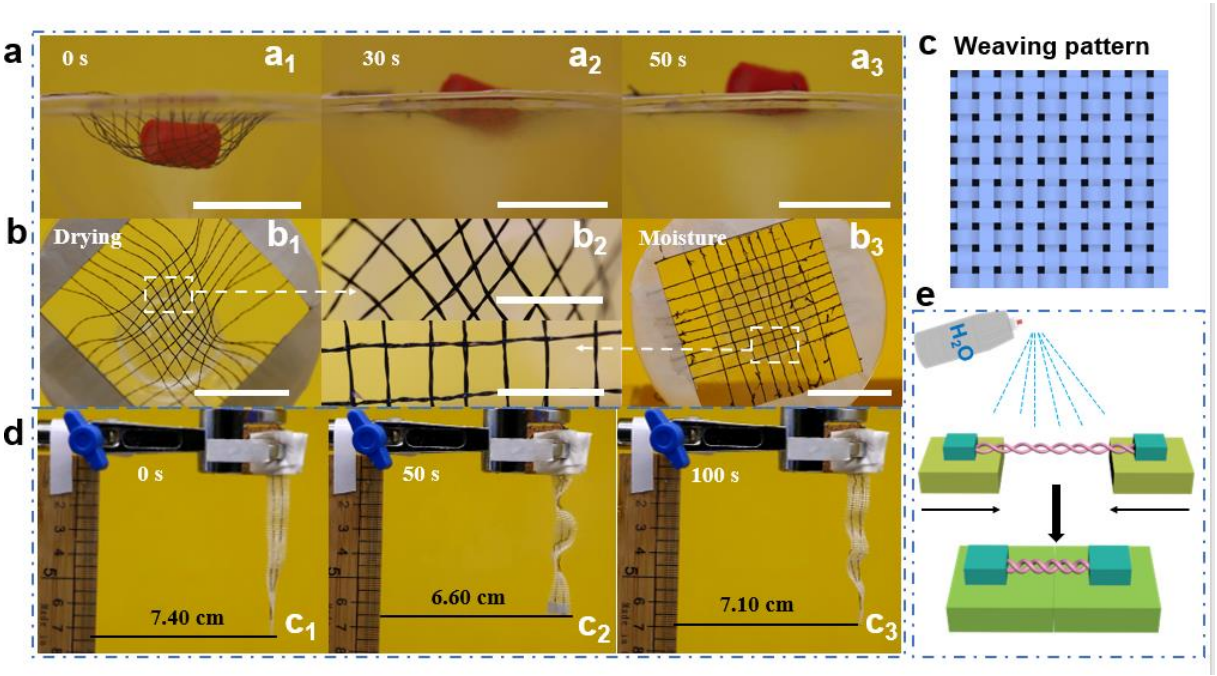

Figure 5. a) Net woven by 9×9 TCY-4 displaying a reversible up-and-down movement under the moisture stimulus. Top view a_1-a_3) and front view b_1-b_3) of the video screenshot of the net during the upward movement. c) The weaving pattern of the smart net. d) The contraction process of fabric woven with two TCY-4. e) Schematic diagram of the actuator promoting the self healing.

This outstanding actuation performance of TCY actuators endowed them with wide-ranging potential applications, including the artificial muscle and smart fabrics. The 9×9 TCYs were sufficiently flexible and robust to be woven directly into a net (**Figure 5a**). The net was suspended and fixed to a frame for further testing. Upon the moisture stimulus, the pendant with a mass of 1.0238 g (20 times heavier than the net) quickly rises 12 mm in height for 45 s (Video S5, Supporting Information). The output gravitational potential energy $W=mgh$ and gravitation potential power $P=W/t$ were calculated to be 2.4 J kg^{-1} and 0.053 W kg^{-1}, respectively. Top view (Figure $5a_1$-$5a_3$) and front view (Figure $5b_1$-$5b_3$) of the video screenshot of the net show the loose and tight net before and after the moisture stimulus. In addition, we demonstrated a smart textile woven from TCY, which responded to humidity change in the environment. The monolayer fabric woven with cotton fibers and two TCY-4 (Figure 5c and

Figure S3, Supporting Information). The weaving pattern of the smart net was shown in Figure 5c. The fabric showed no response to moisture with PTFs due to the elongation of the PTFs and the friction force between PTFs and cotton fibers (Figure S3, Supporting Information). The composite fabric with TCY-4 contracted when stimulated by moisture (Figure 5d Video S6, Supporting Information), which can be used as self-healing (Figure 5e).

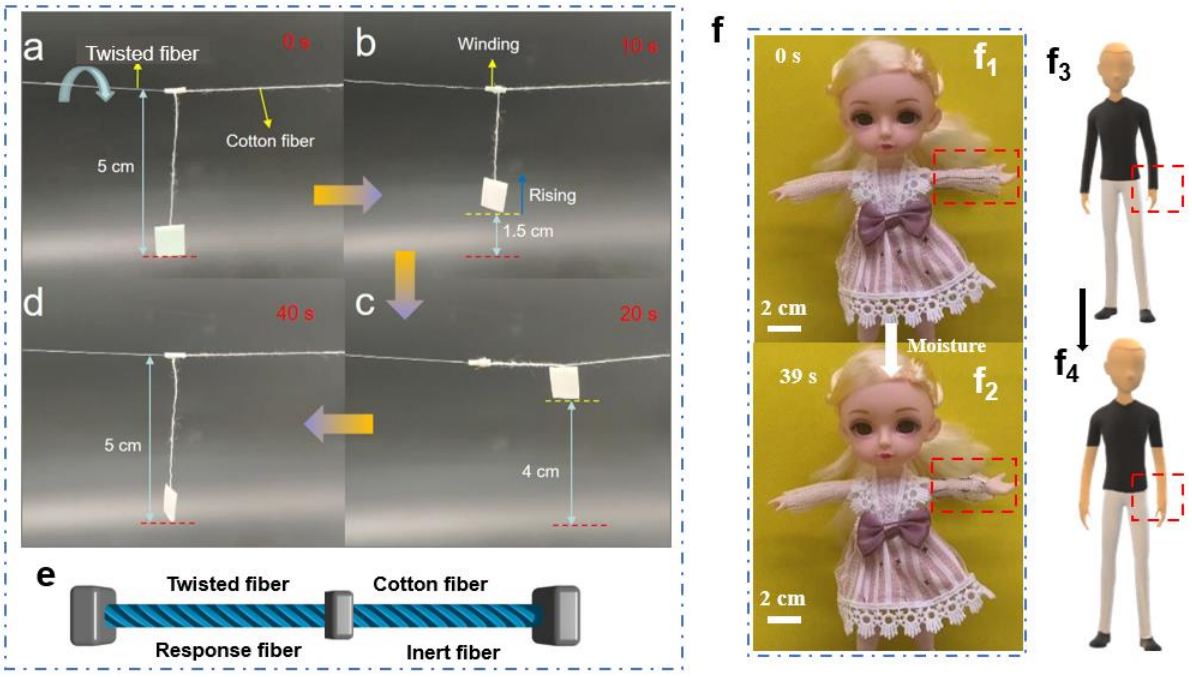

Figure 6. a-d): the lifting process and dropping process of smart crane formed by twisted fiber and cotton fiber when stimulated by moisture. e) Schematic diagram of the smart crane. f_1-f_2) Photos showing sleeves of smart textile contracted when exposed to moisture. f_3-f_4) Schematic diagram of the smart sleeves.

Interestingly, the twisted fiber (active fiber) and cotton fiber (inert fiber) were designed into a simple smart crane, which lifted and dropped a cargo when the fiber were stimulated by moisture and recovered (Figure 6 a-d). The intelligent crane was fabricated by fixing two ends of the twisted fiber (left) and cotton fiber (right) onto a shelf to form a rotating shaft, and the middle part was used to hang a cargo. Figure 6e shows the schematic diagram of the smart carne. As soon as the fiber was stimulated by moisture, a rapid rotation occurred, causing the cargo to

rise rapidly (Figure 6b). Thereafter, the evaporating of the moisture cause the recovery of the fiber, which generated a fast reverse rotation, leading to rapid dropping of the cargo (Fiure 6c). Furthermore, this moisture-responsive textile can change microstructure and macro-shape, hence promising for releasing efficient moisture and thermal management for smart fabric. As can be seen in (Figure 6f), the sleeves of the smart textile shrink in warp (vertical) direction with the increase of humidity (e.g. because of humid or perspiration environment), and expanded with the decrease of humidity. Our smart sleeves exhibited a large contraction upon the exposure to moisture or sweat, and recovered to its initial length as the environment became dry (Video S7, Supporting Information).

3. Conclusion

In conclusion, a TCY-based moisture-driven torsional and shrinkage actuator has been engineered, and can reach the maximum rotation speed of 11400 rpm in 5 s when exposed to moisture, with TCY providing a 9% contraction and delivering a peak work capacity up to 1105.9 J kg-1 upon the increase of RH. The fast water transport arising from MWCNTs, and moisture-triggered in situ hierarchically-twisting process is synergistically responsible for the cascade amplification of the actuation. We also demonstrated the applications of our TCY actuator for moisture-sensitive smart textile. Owing to the high controllability and easy operation of this TCY actuator, coupled with the multifunctionality of MWCNTs, one can envisage the future development towards next-generation autonomous and intelligent device for soft robotics and wearables. This study is the first to suggest the design rationale of the in-situ formation of yarns from primary fibers upon moisture triggers, and provides insight for the innovation of fiber-based actuators.

4. Experimental Section

The detailed materials used, the fiber fabrication and characterization were shown in supporting information.

Supporting Information

Supporting Information is available from the Wiley Online Library or from the author.

5. Acknowledgements

The authors wish to thank the following for financial support: National Natural Science Foundation of China (No. 21104050), a project funded by the Priority Academic Program Development of Jiangsu Higher Education Institutions (PAPD).

Received: ((will be filled in by the editorial staff))
Revised: ((will be filled in by the editorial staff))
Published online: ((will be filled in by the editorial staff))

Table of contents entry

A high-performance hygroresponsive torsional actuator consisting of chitosan and multiwalled carbon nanotubes (MWCNTs) has been engineered via a multi-scale design strategy. The fast transport of water molecules provided by the MWCNTs, the excellent swelling and deswelling behavior of the CS, alongside the in-situ formed hierarchically-assembled twists synergistically contribute to the cascade amplification of moisture-triggered actuation.

Hui Chen, Sunjie Ye, Qianyi Tao, Zhuang Chen, Yingfeng Tu, and Xiaoming Yang*

Hygroresponsive Torsional Yarns and Actuators based on Cascade Amplification of the Deformation

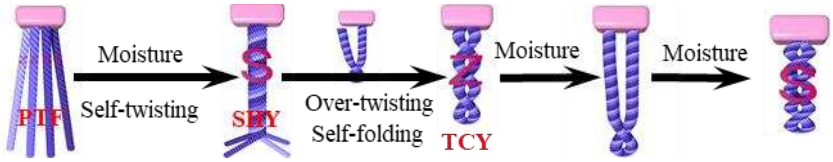

References

[1] E. Reyssat, L. Mahadevan, *J. R. Soc. Interface* **2009**, *6*, 951.

[2] T. D. Wheeler, A. D. Stroock, *Nature* **2008**, *455*, 208.

[3] D. Cosgrove, E. Steudle, *Planta* **1981**, *153*, 343.

[4] J. Dumais, Y. Forterre, *Annu. Rev. Fluid. Mech.* **2012**, *44*, 453.

[5] P. Fratzl, F. G. Barth, *Nature* **2009**, *462*, 442.

[6] J. S. Wang, G. Wang, X. Q Feng, T. Kitamura, Y. L. Kang, S. W. Yu, Q. H. Qin, *Sci. Rep.* **2013**, *3*, 3102.

[7] Z. Zhao, Y. Hwang, Y. Yang, T. F. Fan, J. H. Song, S. Suresh, N. J. Cho, Proc. *Natl. Acad. Sci. U.S.A* **2020**, *117*, 8711.

[8] N. Plaza, S. L. Zelinka, D. S. Stone, J. E. Jakes, *Smart Mater. Struct.* **2013**, *22*, 072001.

[9] Y. Abraham, C. Tamburu, E. Klein, J. W. Dunlop, P. Fratzl, U. Raviv, R. Elbaum, *J. R. Soc. Interface* **2012**, *9*, 640.

[10] W. Jung, W. Kim, H. Y. Kim, Inter. *Comp. Biol.* **2014**, *54*, 1034.

[11] Q. Chen, X. N. Yan, H. Lu, N. Zhang, M. M. Ma, *ACS Appl. Mater. Interfaces* **2019**, *11*, 20473.

[12] N. A. Carter, T. Z. Grove, *J. Am. Chem. Soc.* **2018**, *140*, 7144.

[13] J. Q. Xiong, J. Chen, P. S. Lee, *Adv. Mater.* **2020**, e2002640.

[14] P. N. Chen, Y. F. Xu, S. S. He, X. M. Sun, S. W. Pan, J. Deng, D. Y. Chen, H. S. Peng, *Nat. Nanotechnol.* **2015**, *10*, 1077.

[15] S. S. He, P. N. Chen, L.B. Qiu, B. J. Wang, X. M. Sun, Y. F. Xu, H. S. Peng, *Angew. Chem. Int. Ed. Engl.* **2015**, *54*, 14880.

[16] S. H. Kim, C. H. Kwon, K. Park, T. J. Mun, X. Lepro, R. H. Baughman, G. M. Spinks, S. J. Kim, *Sci. Rep.* **2016**, *6*, 23016.

[17] X. G. Gu, Q. X. Fan, F. Yang, L. Cai, N. Zhang, W. B. Zhou, W. Y. Zhou, S. S. Xie, *Nanoscale* **2016**, *8*, 17881.

[18] H. Chen, Y. H. Ge, S. J. Ye, Z. F. Zhu, Y. F. Tu, D. T. Ge, Z. Xu, W. Chen, X. M. Yang, *Nanoscale* **2020**, *12*, 6104.

[19] Y. H. Ge, R. Cao, S. J. Ye, Z. Chen, Z. F. Zhu, Y. F. Tu, D. T. Ge, X. M. Yang, *Chem. Commun.* **2018**, *54*, 3126.

[20] J. A. Thomas, A. J. McGaughey, *Nano. Lett.* **2008**, *8*, 2788.

[21] J. A. Thomas, A. J. McGaughey, *Phys. Rev. Lett.* **2009**, *102*, 184502.

[22] Y. Q. Zhang, H. Y. Jiang, F. B. Li, Y. H. Xia, Y. Lei, X. H. Jin, G. Z. Zhang, H. J. Li, *J. Mater. Chem. A* **2017**, *5*, 14604.

[23] W. Wang, C. X. Xiang, Q. Z. Liu, M. F. Li, W. B. Zhong, K. L. Yan, D. Wang. *J. Mater. Chem. A* **2018**, *6*, 22599.

[24] H. H. Cheng, Y. Hu, F. Zhao, Z. L. Dong, Y. H. Wang, N. Chen, Z. P. Zhang, L. T. Qu, *Adv. Mater.* **2014**, *26*, 2909.

[25] M. D. Lima, N. Li, M. Jung de Andrade, S. Fang, J. Oh, G. M. Spinks, M. E. Kozlov, C. S. Haines, D. Suh, J. Foroughi, S. J. Kim, Y. Chen, T. Ware, M. K. Shin, L. D. Machado, A. F. Fonseca, J. D. Madden, W. E. Voit, D. S. Galvao, R. H. Baughman, *Science* **2012**, *338*, 928.

[26] M. D. Lima, S. Fang, X. Lepro, C. Lewis, R. Ovalle-Robles, J. Carretero-Gonzalez, E. Castillo-Martinez, M. E. Kozlov, J. Oh, N. Rawat, C. S. Haines, M. H. Haque, V. Aare, S. Stoughton, A. A. Zakhidov, R. H. Baughman, *Science* **2011**, *331*, 51.

[27] B. Fang, Y. H. Xiao, Z. Xu, D. Chang, B. Wang, W. W. Gao, C. Gao, *Mater. Horizons* **2019**, *6*, 1207.

[28] P. N. Chen, S. S. He, Y. F. Xu, X. M. Sun, H. S. Peng, *Adv. Mater.* **2015**, *27*, 4982.

[29] T. Jia, Y. Wang, Y. Dou, Y. Li, M. Jung de Andrade, R. Wang, S. Fang, J. Li, Z. Yu, R. Qiao, Z. Liu, Y. Cheng, Y. Su, M. Minary-Jolandan, R. H. Baughman, D. Qian, Z. Liu, *Adv. Funct. Mater.* **2019**, *29*, 1808241.

[30] S. H. Lin, Z. Wang, X. Y. Chen, J. Ren, S. J. Ling, *Adv. Sci.* **2020**, *7*, 1902743.